The 2009 IEEE/RSJ International Conference on
Intelligent Robots and Systems
October 11-15, 2009 St. Louis, USA

Development of an Elastic Redundant Closed-Loop Robot Manipulator and Its Flexibility Control

Daisuke Matsuura, Nobuyuki Iwatsuki and Masafumi Okada

Abstract—**When hyper redundant robots are used in complex and unpredictable environments such as human living space, they should deal with various contact conditions between surrounding objects. Robots thus should plan and optimize not only applying force to the object but also its distribution among contact area. This paper defines the ability to optimize stiffness distribution of a number of contact points as "Flexibility" and proposes elastic closed-loop mechanism which has a serial chain of revolute joints with torsion coil springs as a lightweight and supple hyper redundant mechanism. Output stiffness is formulated based on the minimization of potential energy, the balancing of internal force and the velocity constraint to construct a closed-loop mechanism. Joint input to obtain both the desired stiffness distribution and desired output position simultaneously is derived from partial derivative of the output stiffness and compensation by a learning control scheme. Motion control experiments with a 10R elastic closed-loop robot demonstrate the effectiveness of the proposed control scheme.**

I. Introduction

Hyper redundant robots that have extremely huge degrees of freedom in the mechanism against their workspaces are expected to be effective in developing dexterous machines that are tended to be used in our living environment, because they can adapt to unpredictable environment by achieving many objectives simultaneously based on redundancy utilization. In the actual use of those robots, contact between robots and their surrounding objects is inevitable under both controlled and uncontrolled conditions, such as manipulation or carrying of arbitrary object, or unpredictable collision with obstacle. To deal with such various situations, a robot should optimize not only positions and velocities of all output links but also output forces and their distribution, applied on contacting object. In addition, output links themselves need to be selectable among entire links of the mechanism according to the current contact condition, to achieve a large adapting capability, instead of those determinately defined.

Manuscript received February 25, 2009. This work was supported in part by Tokyo Institute of Technology, The 21st Century Center of Excellence Program, "Innovation of Creative Engineering through the Development of Advanced Robotics" and the Ministry of Education, Science, Sports and Culture, Grant-in-Aid for Scientific Research (C), 1910592, 2007.

D. Matsuura is with the dept. of Mechanical Engineering, the Ohio State University, Columbus, OH 43210, USA (corresponding author to provide phone: 614-292-8718; fax: 614-292-3163; e-mail: matsuura.12@osu.edu).

N. Iwatsuki is with the dept. of Mechanical Sciences and Engineering, Graduate School of Science and Engineering, Tokyo Institute of Technology, Tokyo 152-8552, Japan (e-mail: nob@mep.titech.ac.jp)

M.Okada is with the dept. of Mechanical Sciences and Engineering, Graduate School of Science and Engineering, Tokyo Institute of Technology, Tokyo 152-8552, Japan (e-mail: okada@mep.titech.ac.jp)

In previous researches aiming to control output force of redundant robots, a number of methods based on force control[1][2], compliance control[3] or impedance control[4][5] have been proposed. However, those methods specify output links beforehand then give desired command values to be achieved, and assumed degrees of freedom are not so many. Thus they are not quite applicable in adaptive contact condition control of hyper redundant robots. Moreover, it is not feasible to compose all active joints by conventional actuators such as electric motors because that will make robot heavier and will slow down the motion. To solve this problem, a part of joint should be composed by elastic elements to secure both large degrees of freedom and lightweight mechanism and to achieve large workspace and large mechanical configuration change. When a redundant robot has elastic joints forming a closed-loop mechanism in contact area, output links can be chosen above that part and output force distribution can be controlled based on the internal force balance. Namely, redundant closed-loop mechanism having elastic joint is effective to perform the above mentioned force distribution control.

This paper proposes "Flexibility Control" concept which represents an ability of hyper redundant robot to achieve a desired force distribution on arbitrary target objects while maintaining the desired output position. A closed-loop redundant mechanism having a serial chain of elastic joints that have torsion coil springs on their rotation axis, is designed to establish the flexibility control scheme. In the formulation of the flexibility control scheme, the output stiffness which describes the relationship between external force acting on each link and mechanical configuration change is formulated as the first step. Then the partial derivative of the output stiffness is employed to obtain the optimum joint input, together with the learning control based on linear combination of error history[6] to achieve both the desired output stiffness distribution and output position at the same time. The established control scheme is applied to motion control experiment of a 10R planar elastic closed-loop robot manipulator.

II. Mechanism Design and Task Definition

Let us consider an elastic closed-loop mechanism shown in Fig.1. The mechanism has two serial chains of active joints called Actuator Part, J_{L1} , ... , $J_{LN\ell}$ and J_{R1} , ... , J_{RNr} , connected to anchor joints respectively. N_ℓ and N_r are the number of active joints in each serial chain. Among the two actuator parts, a serial chain of elastic joints called Spring Part, J_1 , ... ,

J_{Ne}, is attached. Each elastic joint has a torsion coil spring on its rotation axis. Arbitrary links of the spring part can be used as end effectors of the robot, and control points are located on the center of all those links in order to control the distribution of output stiffness. In addition, one of the control points is chosen as an output point of position control. This position control is performed as a main task which should be achieved precisely. The output stiffness distribution control is performed as a sub task which should be achieved as much as possible, next to the main task.

Since M and α are the degrees of freedom of workspace and the constraint condition to construct a closed-loop mechanism respectively, the redundant degrees of freedom that can be used for stiffness distribution control is

$$M_s = N_l + N_r - M - \alpha \,. \tag{1}$$

III. Formulation of the Flexibility Control Scheme

A. Output stiffness analysis

As the first step of the flexibility control formulation, the output stiffness is obtained by iterative optimize calculation. When input angles θ_{L1}, ... , $\theta_{LN\ell}$ and θ_{R1}, ... , θ_{RNr} are given to the actuator parts, the position of each tip of the actuator part is obtained by direct kinematic analysis. Then the mechanical configuration of the spring part is obtained by minimizing potential energy stored in all torsion coil springs of the spring part with respect to spring constant k_i . Since an initial mechanical configuration of the spring part which is geometrically appropriate to form a closed-loop can be obtained after the direct kinematic analysis of the actuator part, potential energy stored in the entire torsion coil springs is written as

$$E = \sum_{i=1}^{N_e} \frac{1}{2} k_i \theta_{Ei}^{\ 2} \,. \tag{2}$$

This potential energy, E, can be minimized based on gradient projection method [7]. When one of the terminals of the spring part, J_1, is assumed to a virtual anchor joint, general solution of joint input of spring part and its partial derivative with respect to joint angle are written as

$$\dot{\boldsymbol{\theta}}_E = \boldsymbol{J}_{Ne}^{\ \#} \dot{\boldsymbol{r}}_{Ne} + \left(I - J_{Ne}^{\ \#} J_{Ne}\right) k \frac{\partial E}{\partial \theta}, \tag{3}$$

$$\frac{\partial E}{\partial \theta} = \left(k_1\theta_1 \quad \cdots \quad k_{Ne}\theta_{Ne}\right), \tag{4}$$

where J_{Ne} is a Jacobian matrix respect to N_e-th joint, the other terminal of the spring part. $J_{Ne}^{\ \#} = J_{Ne}^{\ \mathrm{T}}(J_{Ne}J_{Ne}^{\ \mathrm{T}})^{-1}$ is pseudo inverse of J_{Ne}. $\dot{\boldsymbol{r}}_{Ne}$ is a relative velocity against J_1. A joint input increment to minimize the potential energy, $\dot{\boldsymbol{\theta}}_E$, while holding both terminals of the spring part at the tip of the actuator parts, is obtained by substituting $\dot{\boldsymbol{r}}_{Ne} = 0$ in Eq.(3).

$$\dot{\boldsymbol{\theta}}_E = k\left(I - J_{Ne}^{\ \#} J_{Ne}\right)\left(-k_1\theta_1 \quad \cdots \quad -k_{Ne}\theta_{Ne}\right)^{\mathrm{T}}. \tag{5}$$

The mechanical configuration of the spring part is iteratively refreshed until $\dot{\boldsymbol{\theta}}_E$ become smaller than a threshold ε (=10.0x10^{-10} in below).

From the obtained spring part configuration, the output stiffness of each control point, K_i, can be calculated. Let us consider the i-th control point P_i. The translation of the control point, R_i, caused by an external force, F_i, can be described with respect to the output stiffness as

$$F_i = K_i \Delta R_i \,, \tag{6}$$

where F_i and R_i are M x M matrices defined by M-base vectors as

$$F_i = \left(\boldsymbol{f}_{i,0} \cdots \boldsymbol{f}_{i,M}\right), \; R_i = \left(\boldsymbol{r}_{i,0} \cdots \boldsymbol{r}_{i,M}\right). \tag{7}$$

Since the torque increment of all the joints to balance the external force is written as following equation (8), the external force F_i is derived from its deformation as Eq.(9).

$$\Delta T_E = J_i^{\ \mathrm{T}} F_i \,, \tag{8}$$

$$F_i = \left(J_i^{\ \mathrm{T}}\right)^{\#} \Delta T_E \,, \tag{9}$$

where ΔT_E is a N_E x M matrix, defined by M-base vectors as

$$\Delta T_E = \left(\Delta\boldsymbol{\tau}_0 \cdots \Delta\boldsymbol{\tau}_M\right). \tag{10}$$

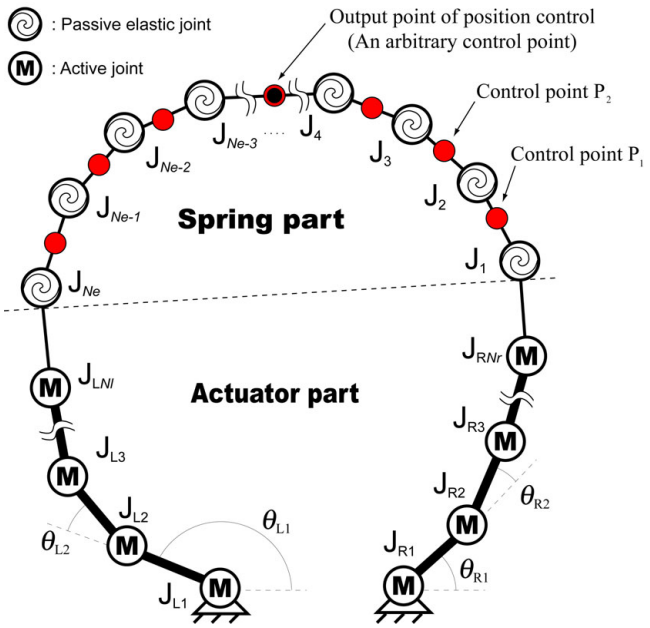

Fig.1 Elastic redundant closed-loop mechanism

Since the torque increment is also expressed by the spring constants and joint angles as

$$\Delta T_E = \mathrm{diag}(k_i)\Delta\Theta_E, \tag{11}$$

the external force F_i can be obtained by substituting Eq.(11) into Eq.(9) as

$$F_i = \left(J_i^{\mathrm{T}}\right)^{\#}\mathrm{diag}(k_i)\Delta\Theta_E, \tag{12}$$

where

$$\Delta\Theta_E = \left(\Delta\boldsymbol{\theta}_0 \cdots \Delta\boldsymbol{\theta}_M\right). \tag{13}$$

By substituting Eq.(12) into Eq.(6), the output stiffness K_i of the control point P_i can be derived as

$$K_i = \left(J_i^{\mathrm{T}}\right)^{\#}\mathrm{diag}(k_i)\Delta\Theta_E\left(J_i\Delta\Theta_E\right)^{-1}. \tag{14}$$

To obtain a proper Jacobian matrix J_i in Eq.(14), a velocity constraint condition should be applied in order to construct a closed-loop mechanism[8]. As illustrated in Fig.2, the spring part can be split into left side part and right side part at the objective control point P_i. At this time, output velocity of the left part and the right part must agree. From this principle, the velocity constraint condition can be written as

$$\Delta\boldsymbol{r}_i = J_{iL}\Delta\boldsymbol{\theta}_L = J_{iR}\Delta\boldsymbol{\theta}_R, \tag{15}$$

where J_{iL} and J_{iR} are Jacobian matrices of the left side part and the right side part respect to P_i, those assumes J_{Ne} and J_1 to temporal anchor joints. Eq.(15) can be decomposed into column vectors and scholar variables, then is organized into two groups, the one is the elements those can be defined freely and the other should be constrained. Since a planar translation is a two-degrees-of-freedom motion, two joint angles are constrained. Eq.(15) can thus be rewritten as

$$\begin{aligned} J_{iL} &= \left[\boldsymbol{j}_{N_e} \quad \boldsymbol{j}_{N_e-1} \quad \cdots \quad \boldsymbol{j}_{i+1}\right], \\ J_{iR} &= \left[\boldsymbol{j}_1 \quad \boldsymbol{j}_2 \quad \cdots \quad \boldsymbol{j}_i\right], \\ \Delta\boldsymbol{\theta}_L &= \left[\Delta\theta_{N_e} \quad \Delta\theta_{N_e-1} \quad \cdots \quad \Delta\theta_{i+1}\right]^{\mathrm{T}}, \\ \Delta\boldsymbol{\theta}_R &= \left[\Delta\theta_1 \quad \Delta\theta_1 \quad \cdots \quad \Delta\theta_i\right]^{\mathrm{T}}, \end{aligned} \tag{16}$$

$$\left[\boldsymbol{j}_{N_e} \quad \boldsymbol{j}_{N_e-1} \cdots - \boldsymbol{j}_1 \quad -\boldsymbol{j}_2 \cdots\right]\begin{bmatrix}\Delta\theta_{N_e}\\ \vdots \\ \Delta\theta_1 \\ \vdots\end{bmatrix} = \left[-\boldsymbol{j}_{i+1} \quad \boldsymbol{j}_i\right]\begin{bmatrix}\Delta\theta_{i+1}\\ \Delta\theta_i\end{bmatrix}. \tag{17}$$

Eq.(17) can be rewritten in a simple form as

$$J_G\Delta\boldsymbol{\theta}_G = J_S\Delta\boldsymbol{\theta}_S, \tag{18}$$

where

$$\begin{aligned} J_G &= \left[\boldsymbol{j}_{N_e} \quad \boldsymbol{j}_{EN_e-1} \quad \cdots \quad -\boldsymbol{j}_1 \quad -\boldsymbol{j}_2 \quad \cdots\right], \quad J_S = \left[-\boldsymbol{j}_{i+1} \quad \boldsymbol{j}_i\right], \\ \Delta\boldsymbol{\theta}_G &= \left[\Delta\theta_{N_e} \quad \Delta\theta_{N_e-1} \cdots \Delta\theta_1 \quad \Delta\theta_2 \cdots\right]^{\mathrm{T}}, \quad \Delta\boldsymbol{\theta}_S = \left[\Delta\theta_{i+1} \quad \Delta\theta_i\right]^{\mathrm{T}}. \end{aligned} \tag{19}$$

The joint angle increment $\Delta\boldsymbol{\theta}_S$ which satisfies the velocity constraint condition is obtained by transforming Eq.(18) as

$$\Delta\boldsymbol{\theta}_S = J_S^{\#}J_G\Delta\boldsymbol{\theta}_G = H\Delta\boldsymbol{\theta}_G = \begin{bmatrix}\boldsymbol{h}_1\\ \boldsymbol{h}_2\end{bmatrix}\Delta\boldsymbol{\theta}_G. \tag{20}$$

where H is a Jacobian matrix which describes the influence of the arbitrary defined element $\Delta\boldsymbol{\theta}_G$ against the constrained elements $\Delta\boldsymbol{\theta}_S$. The composing vectors $\boldsymbol{h}_1$ and $\boldsymbol{h}_2$ are row vectors, size of $(N_e - 2)$. From Eq.(20), each element of $\Delta\boldsymbol{\theta}_s$ that satisfies the closed-loop constraint is obtained as

$$\Delta\theta_{i+1} = \boldsymbol{h}_1\Delta\boldsymbol{\theta}_G, \quad \Delta\theta_i = \boldsymbol{h}_2\Delta\boldsymbol{\theta}_G. \tag{21}$$

From above, the Jacobian matrix which satisfies the velocity constraint condition is obtained as

$$J_i\Delta\boldsymbol{\theta}_E = \left[-J_S \; J_G\right]\begin{bmatrix}\Delta\boldsymbol{\theta}_S\\ \Delta\boldsymbol{\theta}_G\end{bmatrix} = \left[H \; J_G\right]\Delta\boldsymbol{\theta}_G. \tag{22}$$

B. Simultaneous achievement of desired stiffness distribution and output position

A stiffness distribution control is carried out by minimizing the accumulated residual error in-between the desired output stiffness ${}^dK_i$ and actual output stiffness K_i, obtained in Eq.(14). The objective function to be minimized is

$$\phi(\boldsymbol{\theta}_E) = \mathrm{trace}\left({}^dK_i - K_i\right). \tag{23}$$

Angular input for each joint of the spring part to minimize the

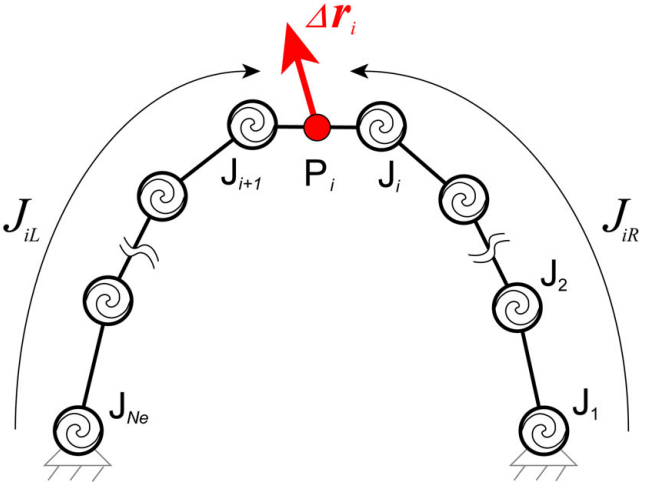

Fig.2 Closed-loop equation around a control point P_i

objective function is obtained from the partial derivative of Eq.(23) with respect to joint angle as

$$\dot{\theta}_i = k\frac{\partial \phi}{\partial \theta} = k({}^dK_i - K_i)\frac{\partial K_i}{\partial \theta}, \tag{24}$$

where

$$\frac{\partial K_i}{\partial \theta} = \left(\frac{\partial J_i}{\partial \theta}\right)\left(k_1\theta_1 \cdots k_{Ne}\theta_{Ne}\right)^{\mathrm{T}} + J_i\left(k_1 \cdots K_{Ne}\right)^{\mathrm{T}}, \tag{25}$$

k (= –0.01 in below) is a negative constant. An angular joint input velocity of the spring part can thus be obtained as

$$\dot{\boldsymbol{\theta}}_E = \left[\cdots \quad \dot{\theta}_i \quad \cdots\right]^{\mathrm{T}}. \tag{26}$$

Since the spring part is a passive mechanism, the obtained joint input cannot be given to the robot directly. Thus the obtained input needs to be converted to tip translation of each actuator part, $\Delta \boldsymbol{r}_1$ and $\Delta \boldsymbol{r}_{Ne}$ as shown in Fig.3, to achieve the desired stiffness distribution. Although an output point of position control that is chosen among a number of control points should be held at a desired position, the stiffness distribution control tends to push the output point out from a desired position. An additional input is thus necessary to keep the output point in position. The learning control scheme based on linear combination of error history[6] is used to achieve this compensation. During the iterative calculation of spring part configuration, the output error of the main task, $\Delta \boldsymbol{e}_{n,j}$, shown as dashed allow in Fig.3, is calculated as

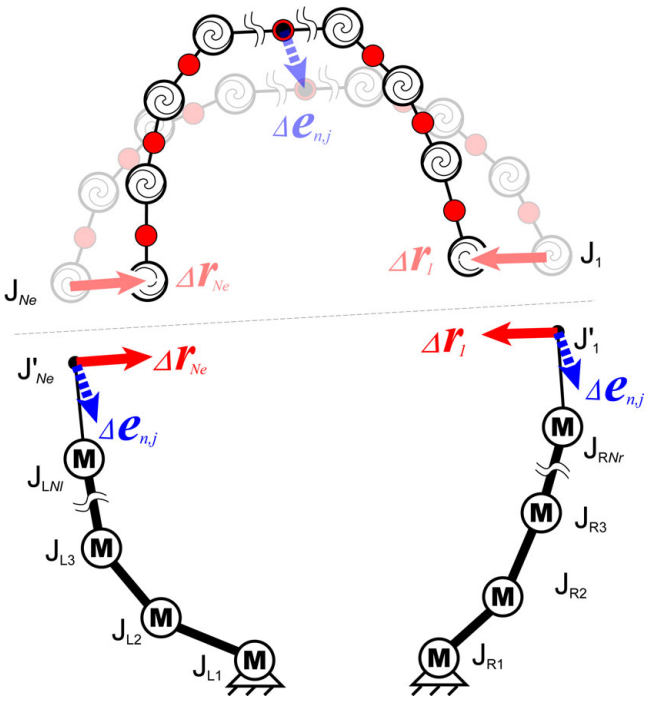

Fig.3 Desired position increment of the stiffness distribution control and

$$\begin{aligned} \boldsymbol{e}_{n-1,j} &= {}^d\boldsymbol{r}_{j-1} - \boldsymbol{r}_{n-1,j}, \\ \boldsymbol{e}_{n-1,j-1} &= {}^d\boldsymbol{r}_{j-1} - \boldsymbol{r}_{n-1,j-1}, \\ \boldsymbol{e}_{n,j-1} &= {}^d\boldsymbol{r}_{j} - \boldsymbol{r}_{n-1,j}. \end{aligned} \tag{27}$$

Where n and j are an iteration count number and a reference point number, which refers the current position of the output point on a desired trajectory, respectively. The obtained errors are stored as output error history so as to calculate the displacement compensation input as

$$\Delta^d\boldsymbol{r}_{n,j} = \Delta\boldsymbol{r}_{n-1,j} + C_0\boldsymbol{e}_{n,j-1} - C_1\boldsymbol{e}_{n-1,j-1} + C_2\boldsymbol{e}_{n-1,j}, \tag{28}$$

where C_0, C_1 and C_2 are learning coefficients ranging $0<C_0, C_2<1$ and $-1<C_1<0$. The actuator joint angle input to achieve this displacement can be obtained as

$$\begin{aligned} \Delta\boldsymbol{\theta}_{Ln,j} &= \Delta\boldsymbol{\theta}_{Ln-1,j} + J_L{}^{\#}\left(C_0\boldsymbol{e}_{n-1,j} + C_1\boldsymbol{e}_{n-1,j-1} + C_2\boldsymbol{e}_{n,j-1}\right), \\ \Delta\boldsymbol{\theta}_{Rn,j} &= \Delta\boldsymbol{\theta}_{Rn-1,j} + J_R{}^{\#}\left(C_0\boldsymbol{e}_{n-1,j} + C_1\boldsymbol{e}_{n-1,j-1} + C_2\boldsymbol{e}_{n,j-1}\right). \end{aligned} \tag{29}$$

The flexibility control is carried out by the simultaneous execution of the stiffness distribution control scheme and the learning control scheme.

IV. Flexibility Control Experiment

A. *Stiffness distribution control*

The proposed flexibility control scheme was validated by experiments with a 10R elastic closed-loop robot shown in Fig.4. The actuator part of this robot is composed of 100mm long links and four actuator units; 5W-output DC motors, optical encoders that generate 512 pulses per revolution and harmonic reducers with a reduction ratio of 100:1. The spring part is a serial chain of six revolute joints connected by 50mm long links. Each of them has a torsion coil spring with a stiffness of 2.0 N·mm/deg. Three control points, P_1, P_2 and P_3 are set on the each center of three links of the spring part.

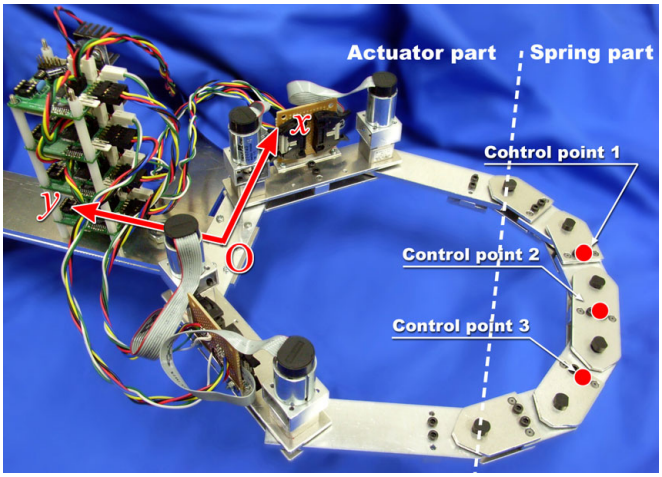

Fig.4 The 10R elastic closed-loop robot

Target stiffness distributions were given to these three control points so as to deal with various contact conditions appropriately.

In the first experiment, only the stiffness distribution control scheme was performed. Three target stiffness distributions those each member is parallel to the y coordinate axis; (i) ${}^dK_1 = {}^dK_3 = (0,1000)$ N/m, ${}^dK_2 = (0,500)$ N/m, (ii) ${}^dK_1 = {}^dK_2 = {}^dK_3 = (0,300)$ N/m and (iii) ${}^dK_1 = {}^dK_3 = (0,10)$ N/m, ${}^dK_2 = (0,1000)$ N/m were given to the robot, then actual output stiffness was measured. A force gauge fixed on a linear stage was used for this measurement. The probe of the force gauge pushed each control point to measure the relationship between the given displacement and reaction force, namely output stiffness. The obtained output stiffness shown in Fig.5 almost agrees to the each target values, except ${}^dK_1$ and ${}^dK_3$ in the setting (iii). In this case, since the output stiffness K_2 was large due to the commanded value, and consequently K_1 and K_3 also become large, almost infinite in the preliminary simulation. This means that some target stiffness settings cannot be achieved when they are extremely large or small. However, the effectiveness of the proposed stiffness control scheme has been confirmed and the elastic closed-loop robot could achieve various stiffness distributions.

B. Object grasping experiment based on flexibility control

In the second experiment, a pair of robots grasped target objects in-between their spring parts to demonstrate the effectiveness of the flexibility control scheme for the achievement of adaptive contact. The target objects were a sponge cube and an octagonal Styrofoam beam, and the above stiffness distributions (i) and (iii) were applied. In this experiment, the center control point P_2 was chosen as an output point of the position control. A desired trajectory, which makes two spring parts closer, was given to grasp the target objects. The stiffness distribution (i) can achieve highly adaptive contact against arbitrary shaped objects because the center contact area stiffness is lower than outside; the distribution (iii) can achieve strong grasping because the output stiffness of entire contact area is high, thus the mechanism becomes rigid against the external force.

Snapshots of the obtained trajectory at the beginning and the end of each grasping motion are shown in Fig.6. The translation and rotation of the target objects after the robot began to contact were measured by image analysis using the vertexes of the polygonal target shape. The obtained translation and rotation are shown in Fig.7. Since the flexibility of the entire system, which includes the target

(i) ${}^dK_1 = {}^dK_3 = (0,1000)$ N/m, ${}^dK_2 = (0,500)$ N/m

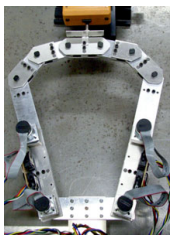

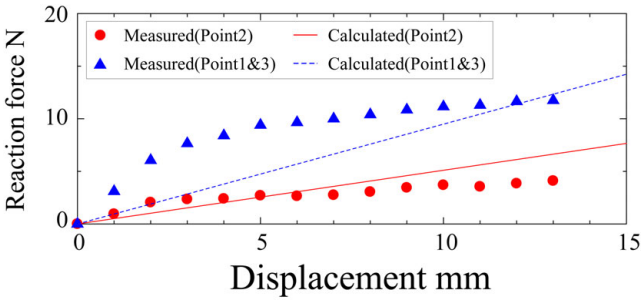

(ii) ${}^dK_1 = {}^dK_2 = {}^dK_3 = (0,300)$ N/m

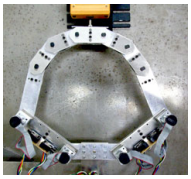

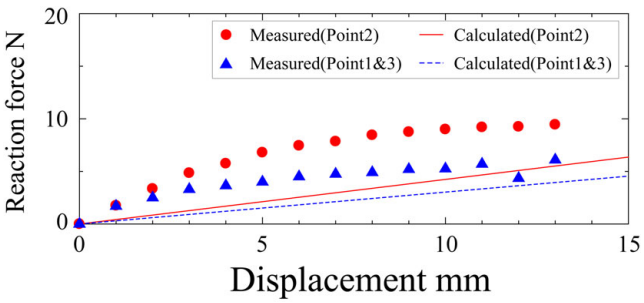

(iii) ${}^dK_1 = {}^dK_3 = (0,10)$ N/m, ${}^dK_2 = (0,1000)$ N/m

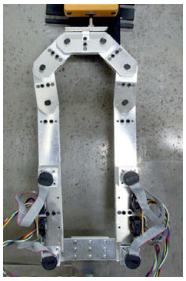

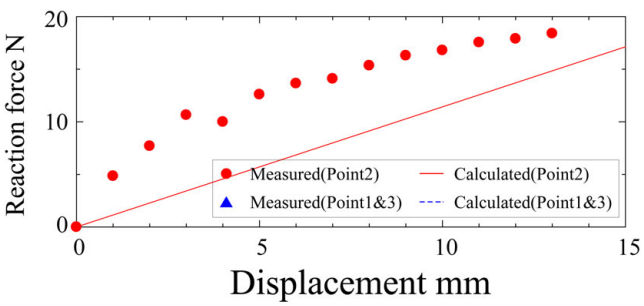

Fig.5 Obtained mechanical configurations (left) and output stiffness distributions (right) by the three target stiffness distribution settings

object and the robot itself, dominates the amplitude of the translation of the object, the sponge cube moved larger than the Styrofoam beam, and it also can be seen that the stiffness distribution (iii) makes the translation distance smaller. Therefore, it can be said that a strong grasping with high stiffness distribution is effective to achieve stable grasping of soft objects. On the other hand, when the robot tried to grasp the Styrofoam beam, reaction of the object became unstable, since unpredictable slip was frequently occurred. This slip appears as a rapid change of the rotation angle in Fig.7, and the fluctuation was smaller when the distribution (i) was applied than in case of distribution (iii). Therefore it can be said that a soft grasping with low stiffness distribution is effective to achieve stable grasping of hard and slippy object because contact force spread out among wide area equally so as to enable a robot to follow arbitrary object shapes.

V. Conclusion

In this paper, "Flexibility Control" concept which enables to control output force distribution and output position simultaneously was proposed. A lightweight and supple elastic redundant closed-loop robot which has a serial chain of elastic joints having a torsion coil spring was designed to realize this concept. The flexibility control scheme was formulated based on the minimization of potential energy stored in each torsion coil spring, the internal force balance among the spring part joints and the learning control scheme based on linear combination of error history. The effectiveness of the proposed control scheme was validated by experiments of stiffness distribution control and object grasping. The robot could achieve a various contact motions adapting to different contact conditions.

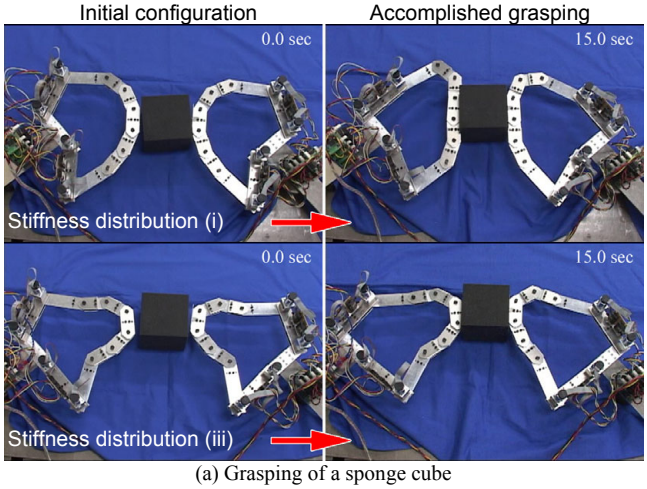

(a) Grasping of a sponge cube

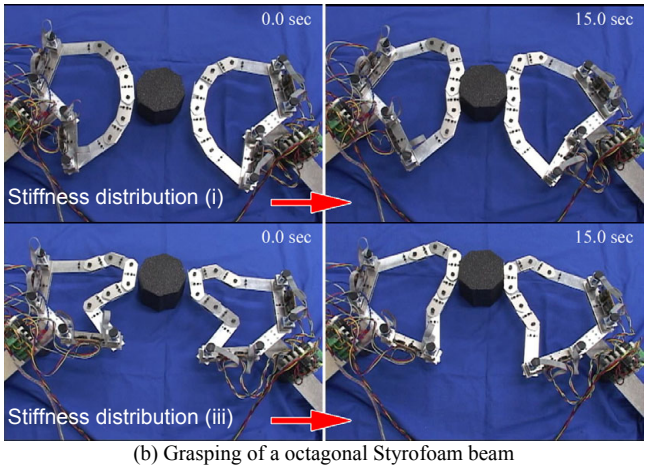

(b) Grasping of a octagonal Styrofoam beam

Fig.6 Snapshots of the output trajectory in the object grasping experiment

References

[1] D. Xiao, B.K. Ghosh, N. Xi and T.J. Tarn: Sensor-Based Hybrid Position/Force Control of a Robot Manipulator in an Uncalibrated Environment, IEEE Transactions on Control Systems Technology, Vol.8, No.4, (2000), pp. 635-645.

[2] B. Nemec and L. Zlajpah: Force Control of Redundant Robots in Unstructured Environment, IEEE transactions on industrial electronics, Vol. 49, No. 1, (2002), pp. 233-2002.

[3] L. Zollo, B. Siciliano, A. De Luca, E. Guglielmelli and P. Dario: Compliance Control for an Anthropomorphic Robot with Elastic Joints: Theory and Experiments, ASME Journal of Dynamic Systems, Measurement, and Control, Vol.127, (2005), pp. 321-328.

[4] A. Albu-Schaffer, C. Ott, U. Frese and G. Hirzinger: Cartesian Impedance Control of Redundant Robots: Recent Results with the DLR-light-weight-arms, Proc. of IEEE International Conference on Robotics and Automation (ICRA03), Vol.3, (2003), pp.3704-3709.

[5] S. Ali, A. Moosavian and M. Mostafavi: Multiple Impedance Control of Redundant Manipulators, Proc. of IEEE Conference on Robotics, Automation and Mechatronics, (2006), pp. 1-6.

[6] D. Matsuura and N. Iwatsuki: Motion Control of Hyper Redundant Robots by Learning Control Based on Linear Combination of Error History and Initial Configuration Optimization with Backward Learning, Journal of Advanced Mechanical Design, Systems, and Manufacturing, Vol.2, No.6, (2008), pp.1011-1020.

[7] R.V.Dubey et al.: An Efficient Gradient Projection Optimization Scheme for a Seven-degree-of-freedom Redundant Robot with Spherical Wrist, Proc. of IEEE Int. Conf. on Robotics and Automation, pp.28-36, 1988.

[8] K. Yamane and Y. Nakamura: Dynamics Computation of Structure-Varying Kinematic Chains for Motion Synthesis of Humanoid, in Proc. of IEEE International Conference on Robotics and Automation, (1999), pp. 714-721.

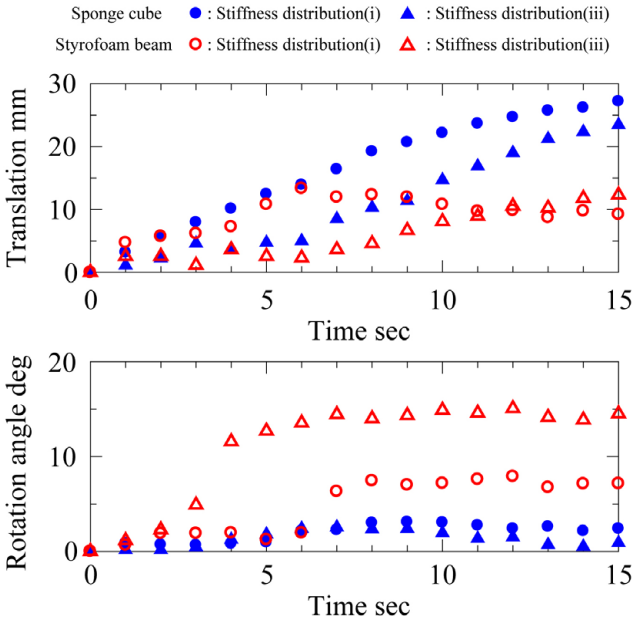

Fig.7 Relative translation (top) and rotation (bottom) of the target object